



## The Synthesis and Electrochemical Properties of Lithium Manganese Oxide ( $\text{Li}_2\text{MnO}_3$ )

Hyoree Seo<sup>a</sup>, Eunah Lee<sup>a</sup>, Cheol-Woo Yi<sup>b,†</sup>, and Keon Kim<sup>a,†</sup>

<sup>a</sup>Department of Chemistry, Korea University, Seoul 136-701, Korea

<sup>b</sup>Department of Chemistry, Sungshin Women's University, Seoul 142-732, Korea

### ABSTRACT :

The layered lithium-manganese oxide ( $\text{Li}_2\text{MnO}_3$ ) as a cathode material of lithium ion secondary batteries was prepared and characterized the physico-chemical and electrochemical properties. The morphological and structural changes of  $\text{MnO(OH)}$  and  $\text{Li}_2\text{MnO}_3$  are closely connected to the changes of electrochemical properties. The crystallinity of  $\text{Li}_2\text{MnO}_3$  is enhanced as the annealing temperature increase, but its capacity is reduced due to the easier structural changes of less crystalline  $\text{Li}_2\text{MnO}_3$  than highly crystalline one. Moreover, the addition of buffer material such as  $\text{MnO(OH)}$  into cathode causes to reduce the morphological and structural changes of layered  $\text{Li}_2\text{MnO}_3$  and increase the discharge capacity and cycleability.

**Keywords:**  $\text{Li}_2\text{MnO}_3$ , manganese oxyhydroxide ( $\text{MnO(OH)}$ ), hydrothermal reaction, structure changes, spinel  $\text{LiMn}_2\text{O}_4$

Received September 17, 2011 : Accepted September 25, 2011

### 1. Introduction

The materials affiliated with lithium transition metal oxides are mainly used for the cathode active materials of the lithium secondary batteries (LIB), and the electrochemical properties are attributed to the oxidation number changes of the transition metal in the active materials. Specifically, the oxidation number of the transition metal ion is changed as lithium ions are inserted and extracted (intercalation/deintercalation), and the average voltage depends on the oxidation/reduction of the each element. However, in the layered structure  $\text{Li}_2\text{MnO}_3$ , the oxidation number of manganese is +4 in the discharging state (lithium ions are intercalated) and is +5 in the charging state (lithium ions are extracted), and therefore, it becomes electrically inactive.<sup>1-2)</sup> However, the recent studies have shown high

capacities by acid treatment which makes deficiencies in the material and induces spontaneous redox reactions or by  $\text{Li}_2\text{O}$  elimination from  $\text{Li}_2\text{MnO}_3$ . It allows Li ions existing between  $[\text{Li}_{1/3}\text{Mn}_{2/3}]$  layers to participate in electrochemical reactions.<sup>3-5)</sup> Moreover, it has been shown that  $\text{Li}_2\text{MnO}_3$ - $\text{LiMO}_2$  ( $M = \text{Mn, Co, Ni, Cr, etc.}$ ) composite electrodes have different polymorphs and reduce structural changes during charge/discharge cycles.<sup>6-7)</sup>

In this study, we investigated physico-chemical and electrochemical properties of the  $\text{Li}_2\text{MnO}_3$  as a cathode material. The  $\text{Li}_2\text{MnO}_3$  is known as an electrical inactive material, but its layered structure was partially changed into spinel structure after charge/discharge cycles. It makes the manganese redox reaction to be possible and allows doing electrochemical activation. In addition, we investigated the role of the  $\text{MnO(OH)}$  as a buffer material for the  $\text{Li}_2\text{MnO}_3$  and discuss the improvement of electrochemical properties.

<sup>†</sup>Corresponding author. Tel.: +82-2-920-7666 (CWY);

+82-2-953-1172 (KK)

E-mail address: cheolwoo@sungshin.ac.kr(CWY);

kkim@korea.ac.kr (KK)

### 2. Experimental

The manganese precursor of  $\text{Li}_2\text{MnO}_3$  is  $\text{MnO(OH)}$

and it is synthesized by hydrothermal reaction. After preparing the mixture of  $\text{KMnO}_4$  (5 g) and ethanol (5 mL) in deionized water (DIW, 400 mL), ~30 mL of stock solution was added into autoclave bomb and performed reaction with stirring at various temperatures (100–150°C) for 24 hours.<sup>8)</sup> The obtained product was washed with DIW and ethanol several times and then dried at 80–100°C for 3 days. To prepare  $\text{Li}_2\text{MnO}_3$ ,  $\text{MnO(OH)}$  and  $\text{LiOH}\cdot\text{H}_2\text{O}$  (Aldrich) were mixed ( $\text{Li} : \text{Mn} = 2.1 : 1$ ), and annealed at the various temperatures (600–900°C) in air atmosphere.

The physico-chemical properties of the samples were characterized by X-ray Diffraction (XRD, Rigaku DMAX-III diffractometer), scanning electron microscopy (SEM, Hitachi S-4300, Japan) and Fourier transform infrared spectroscopy (FT-IR, Nicolet 380). The electrode for the coin cell was prepared using 10 mg of the cathode material, 4 mg of TAB (Welcos) and isopropyl alcohol. The coin cell (CR2032 type) was assembled in Ar-filled glove box and the cell consists of  $\text{Li}_2\text{MnO}_3$ , lithium metal, separator (polypropylene, Welcos) and electrolyte (1 M  $\text{LiPF}_6$  in dimethyl carbonate (DMC)/ethylene carbonate (EC) (1 : 1 v/v), TECHNO Semichem Co.). Charge/discharge tests were performed by WBCS 3000 (WonA Tech, Korea) after aging the coin cell for 10 hours. In order to investigate the structural change of the cathode material after charge/discharge tests, the tested coin cell was disassembled in Ar-filled glove box and dried at room temperature. Then, XRD is measured after washing them with DMC (dimethyl carbonate) for removing  $\text{LiPF}_6$  electrolyte.

### 3. Results and Discussion

The manganese precursor,  $\text{MnO(OH)}$ , of  $\text{Li}_2\text{MnO}_3$  was prepared by hydrothermal reaction method.<sup>8)</sup> The morphology of prepared  $\text{MnO(OH)}$  was investigated by SEM. Fig. 1 shows the SEM images of  $\text{MnO(OH)}$  synthesized at various temperatures. The reaction at the low temperature results in the formation of spherical nanoparticles. The particle size of  $\text{MnO(OH)}$  prepared at 100–120°C is ~70–80 nm. However, the morphology of  $\text{MnO(OH)}$  is significantly different from the reaction at the higher temperature. Fig. 1 (d)–(f) show the SEM images of  $\text{MnO(OH)}$  synthesized at 130–150°C. The shapes of prepared  $\text{MnO(OH)}$  are micro-sized nano-rod (about 100 nm in diameter). The particle size and the degree of agglomeration increase as the reaction temperature rises.

The crystallinity of the prepared manganese precursor,

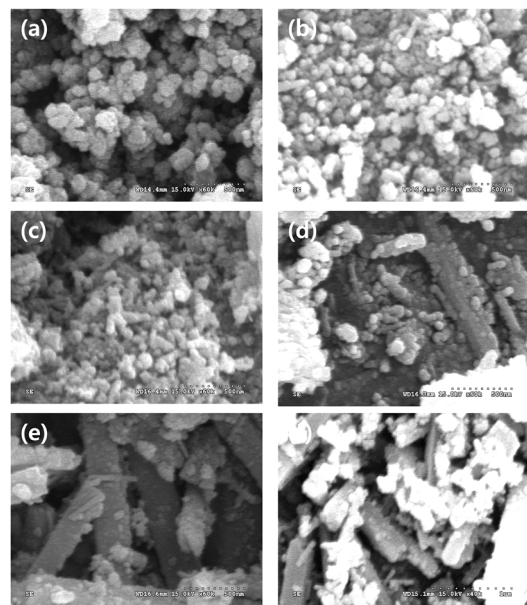


**Fig. 1.** SEM images of  $\text{MnO(OH)}$  synthesized at (a) 100°C, (b) 110°C, (c) 120°C, (d) 130°C (e) 140°C, and (f) 150°C.

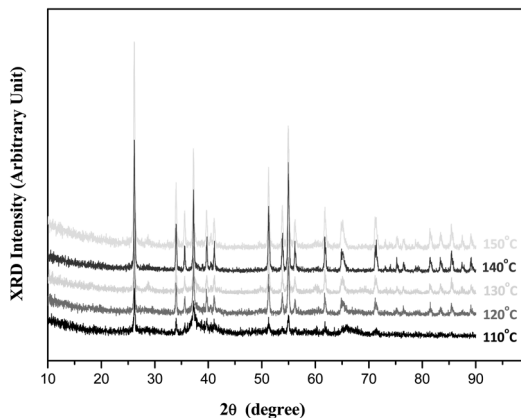


**Fig. 2.** XRD patterns of  $\text{MnO(OH)}$  synthesized at 110–150°C.

$\text{MnO(OH)}$ , is characterized by XRD. Fig. 2 shows XRD results of the sample prepared at various temperatures. The X-ray scattering features of  $\text{MnO(OH)}$  synthesized at 100°C are very broad and not intense due to the formation of nano-sized amorphous particle. However, as the reaction temperature increases, the scattering features become more intense and sharper. It indicates that  $\text{MnO(OH)}$  prepared at high temperature has good crystallinity. In addition, as shown in Fig. 1 (SEM images),

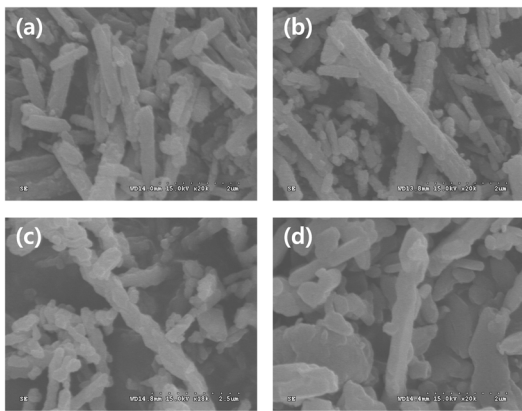


**Fig. 3.** SEM images of  $\text{Li}_2\text{MnO}_3$  synthesized at (a) 600°C, (b) 700°C, (c) 800°C, and (d) 900°C.

because the morphology of  $\text{MnO(OH)}$  has a rod-type shape and large domain as the reaction temperature increases, X-ray scattering features become more intense. The characteristic scattering features are consistent with the published literatures.<sup>8-9)</sup> Even though the minor impurity ( $\text{Mn}_3\text{O}_4$ ) is observed at ~28 and ~60 degrees, it is evident that the as-prepared  $\text{MnO(OH)}$  samples are well crystallized.

In order to prepare  $\text{Li}_2\text{MnO}_3$ , thus-prepared nano-rod shaped  $\text{MnO(OH)}$  synthesized at 140°C was used. The mixture of  $\text{MnO(OH)}$  synthesized at 140°C and  $\text{LiOH-H}_2\text{O}$  (1 : 2.1 mole ratio) was annealed at various temperatures (600–900°C) for 4 hours. Fig. 3 shows SEM images for the prepared  $\text{Li}_2\text{MnO}_3$ . Different from the sample prepared by solid state reaction, the shape of our sample is a rod-type, and this rod-type morphology is the same as that of  $\text{MnO(OH)}$  which we used as the manganese precursor. This phenomenon is called “chimie-douce effect”.<sup>10-11)</sup> The chimie-douce reactions are topotactic reactions that the both of a reactant and product have the equivalent structure, which is the one of the methods to control the shapes of a compound. The synthesized  $\text{Li}_2\text{MnO}_3$  has about 100–150 nm in diameter and micro-sized length similar to the morphology of  $\text{MnO(OH)}$ .

The crystallinity of the prepared  $\text{Li}_2\text{MnO}_3$  samples is investigated by XRD, and the results are shown in Fig. 4. The XRD patterns shown in Fig. 4 indicate that all of the  $\text{Li}_2\text{MnO}_3$  samples prepared at 600–900°C have monoclinic structure. These monoclinic structure peaks are attributed to the cation ordering of  $\text{Li}^+$  and  $\text{Mn}^{4+}$  ions existing in the transition metal layers in the  $\text{Li}_2\text{MnO}_3$ . The charge differences induce a different cation distribution of  $\text{Li}_2\text{MnO}_3$  and simultaneously symmetry lowering from hexagonal

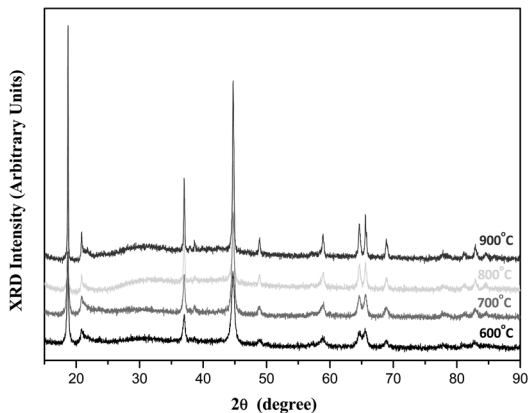


**Fig. 4.** XRD patterns of  $\text{Li}_2\text{MnO}_3$  synthesized at 600–900 °C.

$R\ 3m$  to the monoclinic  $C2/m$ .<sup>1-3)</sup> For the sample annealed at 600°C, the superlattice feature of  $\text{Li}_2\text{MnO}_3$  positioned at ~21 degree completely disappears due to the staking disorder with low crystallinity.<sup>12)</sup> However, the characteristic scattering features of monoclinic structure are clearly seen at 64.5 and 65.5 degree assigned to (135) and (060) reflections even for the sample annealed at low temperature. With further annealing, the scattering features at ~21, 64.5, and 65.5 degree become more intense and sharper as the annealing temperature increases. It indicates that the crystallinity of the  $\text{Li}_2\text{MnO}_3$  is enhanced with an increase in the annealing temperature.

The electrochemical properties of the prepared  $\text{Li}_2\text{MnO}_3$  sample are investigated. The charge/discharge tests are performed at 0.2 C-rate with 2.5–4.5 V cut-off condition. The results of charge/discharge tests are shown in Fig. 5. From the results of the charge/discharging tests, discharge capacities monotonically increase as the number of cycle increases, and it decreases after a certain maximum point. It can be explained that these rapid changes are contributed to the irreversible phase transition.<sup>13-14)</sup> The results of the cell with  $\text{Li}_2\text{MnO}_3$  annealed 600°C show relatively stable capacities and the difference between the minimum and the maximum discharge capacities is the smallest among the samples annealed at various temperatures. The cell with  $\text{Li}_2\text{MnO}_3$  annealed at 700°C shows the best maximum discharge capacity which is larger than that of the sample annealed at 600°C. However, the initial capacity is smaller than the sample annealed at 600°C. On the other hands, the cells with  $\text{Li}_2\text{MnO}_3$  annealed at 800 and 900°C show the significantly low initial discharge capacities, but their cycleabilities are improved with respect to the cells with

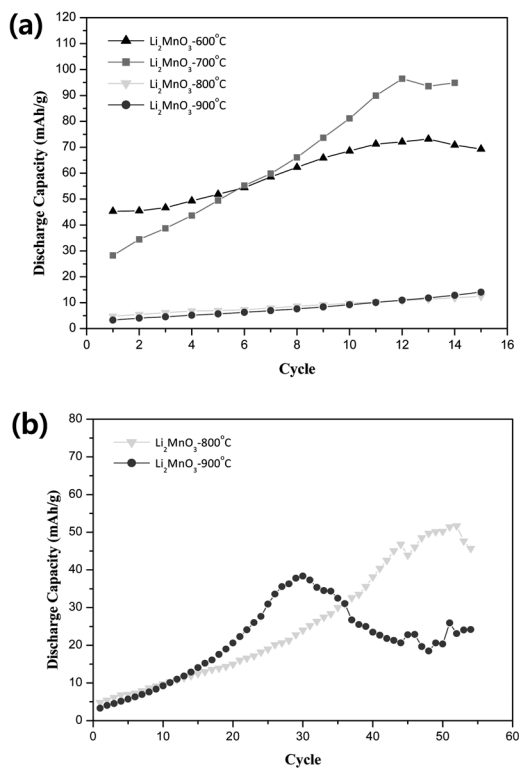


Fig. 5. Discharge capacities of (a)  $\text{Li}_2\text{MnO}_3$  synthesized at 600-900°C cells (after 15cycles) and (b)  $\text{Li}_2\text{MnO}_3$  synthesized at 800 and 900°C (after 54cycles).

$\text{Li}_2\text{MnO}_3$  annealed at 600 and 700°C. Practically, the stoichiometric  $\text{Li}_2\text{MnO}_3$  shows no electrochemical reactions because it is difficult for the lithium ions to diffuse into the Mn layer. Hence, the lithium ion diffusion is probably enhanced in less crystalline particles. Even if the maximum discharge capacities of the samples annealed at various temperatures are different for the annealing temperature, the overall change of the discharge capacity for the different samples follows the same trend. It means that structural change of the active materials, annealed at different temperature, follows the same mechanism during the repeated lithium ion intercalation/deintercalation processes. To investigate the structural change after cell tests, the cathodes of the tested cells were washed with DMC, dried and then performed the X-ray diffraction experiments. Fig. 6 shows the XRD results of the cathode material after cell tests. As shown in the figure, the superlattice scattering features of the layered structure  $\text{Li}_2\text{MnO}_3$  at ~21 degree completely disappears and one of the pair of the monoclinic features at ~65.5 degree significantly reduced. It is evident that the layered structure of the rock-salt  $\text{Li}_2\text{MnO}_3$  partially collapsed.<sup>3)</sup> Besides the change of main feature, some minor scattering feature appears at ~40 and ~58 degree after the cell test. These minor scattering features are assigned to spinel  $\text{LiMn}_2\text{O}_4$ . Hence, the rock-salt  $\text{Li}_2\text{MnO}_3$  gradually changes the structure to spinel  $\text{LiMn}_2\text{O}_4$  and this result is consistent with previous publication.<sup>15)</sup> Due to the influences of the  $\text{Mn}^{3+}$  of thus-

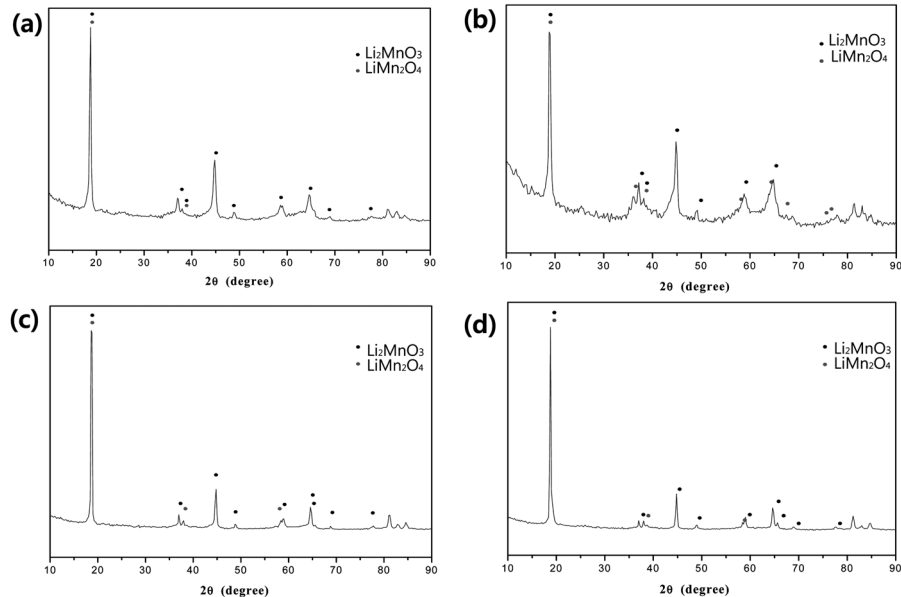
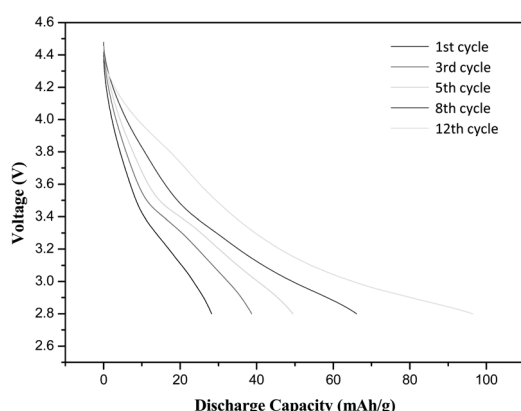


Fig. 6. XRD data for structure changes after cycle tests of  $\text{Li}_2\text{MnO}_3$  synthesized at (a) 600°C, (b) 700°C, (c) 800°C, and (d) 900°C.

formed  $\text{LiMn}_2\text{O}_4$ , the transition between manganese ions with +3/+4 oxidation numbers is probably possible, and therefore, electrochemically inactive  $\text{Li}_2\text{MnO}_3$  becomes active as well as increases the discharge capacity. Therefore, the low crystalline  $\text{Li}_2\text{MnO}_3$  annealed at the lower temperature, having high stacking fault rate,<sup>16)</sup> shows relatively high discharge capacities due to the easier structural changes than highly crystalline  $\text{Li}_2\text{MnO}_3$  annealed at the high temperature. Moreover, because the structure changes of well-crystalline  $\text{Li}_2\text{MnO}_3$  annealed at 800 and 900°C are proceeded slowly, it probably takes longer time to reach the state that the redox reactions of the manganese can be activated. In order to elucidate the transition between manganese ions with +3/+4 oxidation numbers, the discharge capacity - voltage curves of  $\text{Li}_2\text{MnO}_3$  annealed at 700°C are plotted in Fig. 7. At the initial several cycles, ~4.0 V plateau related to the manganese +3/+4 redox reaction is too short. However, as increasing the number of cycle, the plateau range around 4.0 V gradually increases and the total discharge capacity is enhanced corresponding to the results as mentioned above.

As already mentioned, the layered  $\text{Li}_2\text{MnO}_3$  experiences the structural changes as charge/discharge cycles proceed. In order to reduce the morphological and structural change of this cathode material,  $\text{MnO(OH)}$  used as the manganese precursor is blended with layered  $\text{Li}_2\text{MnO}_3$ . The spherical  $\text{MnO(OH)}$  nano-particle prepared at 100°C probably acts as a buffer against the morphological and structural change of layered  $\text{Li}_2\text{MnO}_3$  because  $\text{MnO(OH)}$  nanoparticle not only has the smaller particle size than layered



**Fig. 7.** Structure changes of each  $\text{Li}_2\text{MnO}_3$  after cycle tests at 2nd, 5th, 8th, and 12th cycles; (a) Discharge capacities of  $\text{Li}_2\text{MnO}_3$ -700°C at the each step and (b) XRD data of the  $\text{Li}_2\text{MnO}_3$ -700°C cell after cycle tests at the each step.

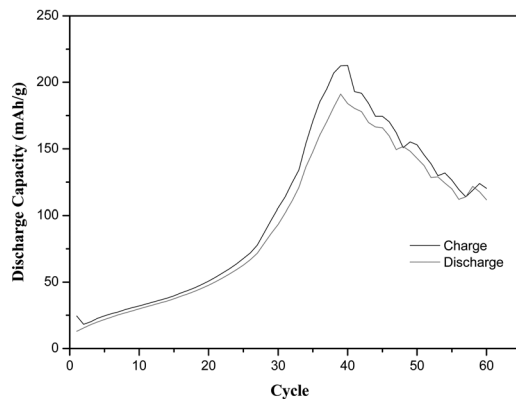


**Fig. 8.** Charge/discharge performances of the  $\text{Li}_2\text{MnO}_3$ - $\text{MnOOH}$  composite.

$\text{Li}_2\text{MnO}_3$  but also is converted to an active material, lithium manganese oxide, after intercalation of lithium ion into  $\text{MnO(OH)}$ . To prepare the cathode,  $\text{MnO(OH)}$  synthesized at 100°C and  $\text{Li}_2\text{MnO}_3$  (1 : 1 mole ratio) are mixed to make an active material. The charge/discharge tests are performed to investigate the electrochemical property and the results are shown in Fig. 8. The overall cycle performances show the volcano shapes for the discharge capacity with a maximum point, and the initial capacities are gradually increased. However, unlike the case that  $\text{Li}_2\text{MnO}_3$  is used alone, the maximum discharge capacity is greatly enhanced and appears at ~40th cycle. It demonstrates that the structural changes from layered to spinel are slowly proceeded by the addition of  $\text{MnO(OH)}$  as a buffer. It also indicates that the slow structural changes during lithium-ion intercalation/deintercalation can be occurred and increases the capacities.

#### 4. Conclusion

We synthesized the manganese oxyhydroxide ( $\text{MnO(OH)}$ ) by hydrothermal reaction and  $\text{Li}_2\text{MnO}_3$  cathode material was prepared by solid-state reaction of  $\text{LiOH}$  with as-prepared  $\text{MnO(OH)}$ . The electrochemical performances and structural changing properties of the electrochemically inactive and layered  $\text{Li}_2\text{MnO}_3$  was investigated. The prepared  $\text{MnO(OH)}$  shows different morphologies and crystallinity as a function of reaction temperature. However, the morphology of  $\text{Li}_2\text{MnO}_3$  is not significantly changed with an increase in the annealing temperature, and it has the same morphology as the manganese precursor,  $\text{MnO(OH)}$ . The crystallinity of

$\text{Li}_2\text{MnO}_3$  is enhanced as the annealing temperature increases, but its capacity is reduced due to the easier structural change than highly crystalline  $\text{Li}_2\text{MnO}_3$  annealed at the high temperature. The layered structure of the  $\text{Li}_2\text{MnO}_3$  is partially changed into  $\text{LiMn}_2\text{O}_4$  spinel structure after charge/discharge cycles and the electrochemical properties are enhanced because the manganese redox reaction in the  $\text{Li}_2\text{MnO}_3$  can be possible. Moreover, the addition of buffer material such as  $\text{MnO(OH)}$  into cathode causes to reduce the morphological and structural changes of layered  $\text{Li}_2\text{MnO}_3$  and increases the discharge capacity and cycleability.

### Acknowledgements

This study was supported by HANARO center of Korea Atomic Energy Research Institute and Korea and Korea Ministry of Education, Science & Technology (MEST), Korean government, through its National Nuclear Technology Program.

### References

- S.H. Park, Y. Sato, J.K. Kim and Y.S. Lee, *Mater. Chem. Phys.*, **102**, 225 (2007).
- M. Tabuchi, K. Tatsumi, S. Morimoto, S. Nasu, T. Saito and Y. Ikeda, *J. Appl. Phys.*, **104**, 043909 (2008).
- J.K. Ngala, S. Alia, A. Doble, V.M.B. Crisostomo and S.L. Suib, *Chem. Mater.*, **19**, 229 (2006).
- A.D. Robertson and P.G. Bruce, *Chem. Mater.*, **15**, 1984 (2003).
- P.G. Bruce, A.R. Armstrong and R.L. Gitzendanner, *J. Mater. Chem.*, **9**, 193 (1999).
- X.K. Huang, Q.S. Zhang, H.T. Chang, J.L. Gan, H.J. Yue and Y. Yang, *J. Electrochem. Soc.*, **156**, A162 (2009).
- S.S. Shin, Y.K. Sun and K. Amine, *J. Power Sources*, **112**, 634 (2002).
- W.X. Zhang, Y. Liu, Z.H. Yang, S.P. Tang and M. Chen, *Solid State Commun.*, **131**, 441 (2004).
- T. Gao, F. Krumeich, R. Nesper, H. Fjellvag and P. Norby, *Inorg. Chem.*, **48**, 6242 (2009).
- F. Capitaine, P. Gravereau and C. Delmas, *Solid State Ionics*, **89**, 197 (1996).
- S.L.S. Doron Levin, and Jakie Y. Ying, *American Chemical Society*, **622**, 237 (1996).
- A. Boulineau, L. Croguennec, C. Delmas and F. Weill, *Solid State Ionics*, **180**, 1652 (2010).
- P. Kalyani, S. Chitra, T. Mohan and S. Gopukumar, *J. Power Sources*, **80**, 103 (1999).
- Y. Sun, Y. Shiosaki, Y. Xia and H. Noguchi, *J. Power Sources*, **159**, 1353 (2006).
- M.H. Rossouw and M.M. Thackeray, *Mater. Res. Bull.*, **26**, 463 (1991).
- L. Croguennec, P. Deniard and R. Brec, *J. Electrochem. Soc.*, **144**, 3323 (1997).